MECHANICAL RESPONSE OF A VASCULAR SELF-HEALING CEMENTITIOUS MATERIAL SYSTEM UNDER VARYING LOADING CONDITIONS

Selvarajoo T, Davies RE, Freeman BL and Jefferson AD

ABSTRACT

The paper presents results from two groups of experimental tests on a pressurised vascular self-healing cementitious material system, in which low viscosity cyanoacrylate was employed as the healing-agent. The first group comprised three series of tests on plain concrete notched prismatic beams. These tests examined the effects on the mechanical response of varying the healing period, the rate of loading and the healing-agent pressure. The second group involved two series of direct tension tests on doubly notched prismatic specimens, each of which had a different crack opening displacement during the healing period. In this second group of tests, healing was allowed to take place in cracks that were held stationary for a period of time, with the degree of mechanical healing being measured for different healing periods. The paper also presents a simplified damage-healing model that is used to interpret the test results and to bring clarity to the indices used to evaluate the degree of healing. The tests were designed to provide new data on simultaneous damage-healing behaviour as well as on the effects of varying pressure, static healing periods and cracking configurations on the mechanical response of this self-healing cementitious material (SHCM) system. These data have been used to guide the development of a new numerical model for SHCMs (reported elsewhere) and should be useful to others who are developing design procedures and/or computational models for similar material systems.

1. INTRODUCTION

This paper presents the results from a series of tests on an autonomic self-healing cementitious material (SHCM) system. The main motive for exploring such self-healing (SH) systems lies in the need to improve the durability of structures formed from cementitious materials [1], as elucidated in a number of recent review papers [2–4]. Much previous work on SHCMs has focussed on concrete, although SH systems have also been successfully applied to other cementitious materials such as mortar [5–7], fibre reinforced concrete [5,8] and engineered cementitious composites (ECCs) [9].

The efficacy of cementitious SH systems that employ autonomic healing-agents has been demonstrated in a number of studies over the past 25 years (e.g. [6,10–14]). A range of healing-agents have been employed in these systems, including; cyanoacrylate (CA), that polymerises upon contact with moisture within the cementitious matrix [6,9,15,16]; sodium silicate, which reacts with the Portlandite in the cementitious matrix [11,17–20]; polyurethane (PU) that has been applied as a doubly encapsulated two-component agent comprising a prepolymer and accelerator [21–23] and as a single component agent [23–26]; methyl methacrylate (MMA), which was originally employed in a three-component system by Dry and McMillan [27] but which was later developed by Van Tittelboom et al. [28] as a two-component system that used compounds of MMA monomer with an initiator and MMA with an activator; as well as epoxy resins, which have been tested in a doubly encapsulated two-part system [29] but which have also been tested as a singly encapsulated compound (CAP) with a dispersed hardener or with functionalised silica nanoparticles [30,31].

There are considerable differences in the way that these agents interact and form bonds with the cementitious matrix. Low viscosity autonomic agents, such as CA, have been shown to permeate into the micro-cracked zone adjacent to a macro-crack as well as to fill the crack itself. The agent forms chemical bonds with the cementitious matrix and -in the micro-cracked zone- forms a cementitious-polymer composite which is significantly stronger than the virgin cementitious matrix [6]. By contrast, there are other agents that react with the cementitious products of the matrix; for example, sodium silicate solution (SSS) reacts with calcium hydroxide (CH) to form a Calcium Silicate Hydrate (C-S-H) gel within cracks [11,17-20], which then develops bonds with the surrounding material. The latter process (SSS) is considerably slower

than the former (CA) but has the advantage that the bonding material is naturally compatible with the concrete or mortar.

The methods used to deliver healing-agents to micro-cracked or macro-cracked regions of the cementitious matrix may be broadly categorised as encapsulation-based systems and vascular-based systems. The former encompasses systems that use micro-capsules [32–36], glass and ceramic macro-capsules [6,9,21–24,37,38], cementitious hollow tubes [39], hollow fibres [9,40] and polymeric tubes [14]. In the latter category, vascular channels are created by either casting breakable tubes into the cementitious matrix [6,15,41], embedding cementitious tubular channels [13], casting and then removing metal rods [42] or flexible polymer tubes [43], or embedding 3D printed vascular networks [13].

The majority of the above delivery systems rely on capillary forces to draw the healing-agents into cracks [2,5] but some investigators have pressurised vascular networks to promote the flow and delivery of the healing-agent [44]. Another mechanism for boosting healing-agent transport is to employ healing-agents that foam [13,21].

Much fuller accounts of previous work on autonomic cementitious self-healing material systems have been provided in a number of review articles [2,4,5,45,46].

The effectiveness of the above self-healing material systems has been evaluated using a range of different test methods and imaging techniques [45]. Amongst these, the most widely-used method for evaluating the degree of mechanical healing is to employ beam specimens under either three point (e.g. [6,12,47]) or four-point loading (e.g. [9,24,48]). The majority of four-point tests have been applied to fibre reinforced self-healing materials and used to explore the healing of distributed micro-cracks, whereas notched three-point tests have more frequently been applied to autonomic systems in unreinforced specimens [45].

Very few investigators have employed direct tension tests to investigate mechanical healing in unreinforced specimens due to the difficulty of controlling such tests. An exception to this is the work of Gilabert et al. [23] who conducted direct tension tests on assembled concrete specimens, which had tubes of PU crossing a preformed planar opening. Gilabert et al.'s work evaluated healing indices, but their testing arrangement was not designed to achieve stable post-peak responses. Direct tension tests have been used by others to investigate the change in flow properties due to healing in fibre reinforced materials, for which the post-peak responses tend to be more stable [45].

Compression tests on cementitious material specimens, that produce a diffuse array of micro-cracks, have been used to evaluate healing but this type of test has most frequently been applied to weaker materials, including a biomimetic Portland cement mortar [49] and a range of lime mortars [7].

Increasing use has been made of imaging techniques to explore internal crack patterns and the morphology of healed zones of material (e.g. [20,24,45,49]). These imaging techniques can provide considerable insight into the behaviour of healing systems, but they have not yet been applied to capture real-time damage and healing processes.

A fuller review of characterisation and imaging techniques applied to self-healing cementitious materials has been provided by Ferrara et al. [45].

Most of the work referred to above has been aimed at proving the efficacy and/or characterising the properties of SH systems. Much less experimental work has been directed towards the specific requirements of design and numerical models for a range of loading scenarios [3,45]. The lack of a comprehensive data set for any one autonomic healing system became evident to the authors whilst writing a review of numerical models for self-healing cementitious materials [3] and during the development of the new numerical model described in Reference [50]. Thus, the aim of the present research programme was to gather a consistent new set of data on healing-agent transport, curing and mechanical healing for a range of loading rates that could be used to develop numerical and design models for autonomic self-healing cementitious material systems.

The specific objectives of the present programme of work were, for a selected autonomic self-healing system, to (i) characterise the flow and curing properties, (ii) understand the healing mechanisms, (iii) quantify transient healing behaviour under different loading conditions, (iv) evaluate the benefits of

pressurising the healing agent and (v) bring clarity to be meaning of healing indices by relating them to a damage-healing model. The work on flow and curing properties is reported in a linked paper [51], with key results being summarised in Appendix B of this paper. The results of the experiments and theoretical studies that address objectives (ii) to (v) are reported in this paper.

The self-healing system selected for this study used cyanoacrylate as the healing agent and channels cast into the cementitious matrix for the delivery of the agent. This system has already been shown to give significant healing in relatively short time periods [6,43,44] and was thus considered suitable for the current testing programme. It is emphasised that the aim of the work was not to prove the efficacy of this system, which has already been done, but to address the above aim and individual objectives.

The structure of the remainder of this paper is as follows;

- Section 2 describes the selected self-healing system and gives details of the materials used in the study;
- Section 3 describes the experimental programme, gives details of the experimental procedures and describes the testing arrangements;
- Section 4 presents a one-dimensional damage-healing model that is used to help interpret the experimental data and to clarify the meaning of certain healing indices;
- Section 5 presents the experimental results, along with some discussion and specific conclusions from each group of tests;
- Section 6 draws some overall conclusions from the study.

2. VASCULAR SYSTEM AND MATERIALS

2.1 Vascular healing system

A vascular system was selected because it allows the healing-agent to be externally pressurised and because the supply of agent can be carefully controlled. The generic vascular healing system used for the present experimental programme is illustrated in Fig. 1. The flow channels shown in the figure were formed using the method proposed by Davies et al. [43,44], which involves casting 4mm diameter flexible polyurethane terephthalate (PET) tubes into the specimens and subsequently removing them when the concrete has cured for one day.

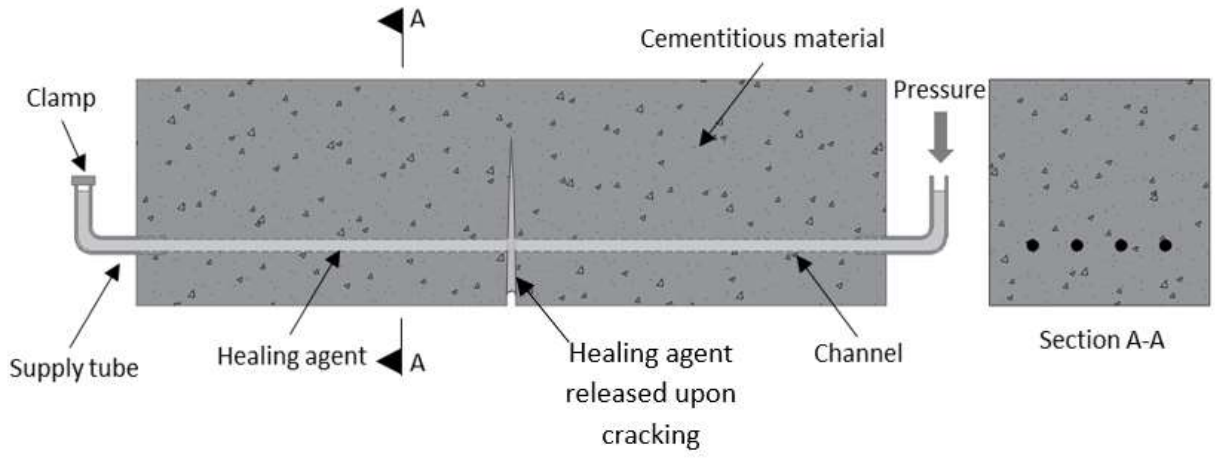

Fig. 1. Generic autonomic healing system

2.2 Materials

2.2.1 Healing-agent

Cyanoacrylate (CA) [52] was chosen as the healing-agent because it heals cracks with openings from 0.1 to 0.5mm in a period of seconds or minutes [6], with the time depending on the crack opening (i.e. the thickness of the adhesive layer) [53]. This choice facilitated the relatively large experimental programme of

work because damage-healing behaviour could be captured in experiments that had durations of minutes (1 to 10 mins). Fast-acting agents, such as CA, have been explored by several investigators [6,9,15,16,27]. They are applicable to structures subject to significant dynamic loading, such as coastal, offshore and bridge structures. Such situations require a fast-acting agent because cracks can open and close many times within the curing period of a slower-acting agent (e.g. sodium silicate) [54,55]. The associated disturbance of a body of slow-acting healing-agent would prevent stable bonds from forming and healing from taking place.

The properties of the CA used in this study [51,52] are given in Table 1.

Table 1. CA properties

γ (N/m)	ρ_h (kg/m^3)	μ (Ns/m^2)	θ_s (rad)	f_{CA} N/mm^2
0.034	1060	0.004	0.175	21

Notes: γ is the surface tension, ρ_h is the density, μ is the viscosity, θ_s is the static contact angle and f_{CA} is the tensile strength of CA.

More information on the flow and curing properties of the CA used in this study are given in the linked paper [51], the key parameters and models from which are given in Appendix B.

The fact that the tensile strength of CA is greater than that of the concrete for this study means that healed strengths were not governed by the tensile strength of CA.

The use of CA in unsealed structural members in buildings would cause some health and safety concerns because it is highly reactive and bonds human skin; however, the aim of this work is not to prove the practicability or sustainability of CA as a healing agent but to provide data that can be used to develop design and analysis models for autonomic healing systems.

2.2.2 Concrete and curing regime

The mix properties of the concrete used to form all cementitious specimens are given in Table 2.

Table 2. Concrete mix properties

Cement type	Ordinary Portland Cement (CEM II/A-L 32, 5R)
Coarse aggregate type	Crushed limestone
Fine aggregate type	Crushed marine sand with limestone
Mix proportions	470 kg/m^3: 986 kg/m^3: 728 kg/m^3: 216 kg/m^3 (cement: coarse aggregate: fine aggregate: water) with a maximum aggregate size of 10mm

A slump test was undertaken for every batch of concrete prepared for the tests reported in this paper. In addition, three cubes and three cylinders were cast and then tested on the same day as the main test specimens i.e. at an age of 8 days (see the curing regime below). The mean and CoV values given below are based on all of these tests.

Table 3. Plastic and hardened concrete properties

Property	Mean	CoV %
Slump [1]	120 (mm)	6
f_{cu}	39.4 (N/mm^2)	5.2
f_{cyl}	3.4 (N/mm^2)	10.2

Notes: the slump tests were in accordance with BS EN 12350-2:2009: f_{cu} = concrete compressive cube strength measured using 100mm specimens ; f_{cyl} = concrete cylinder splitting strength measured using 100x200mm (diameter x height) specimens.

It is generally accepted that the true tensile strength (f_t) is approximately 0.85 f_{cyl}, (i.e. f_t = 0.85 f_{cyl}) and the true uniaxial strength (f_c) is approximately 0.8 f_{cu} (i.e. f_c = 0.8 f_{cu}) [56].

All specimens were cast, demoulded after 1 day, immersed in water for 5 days, oven dried at 90°C for 1 day and then allowed to cool at room temperature for one further day prior to testing.

A nominal specimen age of eight days was chosen to facilitate the large testing programme and because neither the absolute strength of the specimens nor the degree of hydration of the concrete was critical to establishing the autonomic self-healing characteristics. In addition, concrete is normally loaded and experiences its first cracking when it is few days old. Therefore, for the present work, it was inappropriate to use the customary 28 days of curing.

An oven temperature of 90^{o}C was selected to remove most of the capillary water. At this temperature, little or no thermal damage would be expected [57] and any minor changes that this heating caused to the structure of the cementitious matrix would not have significantly affected the damage-healing responses. The main reason for drying the specimens was to minimise any potential interaction between the CA self-healing-agent and any excess capillary water, and thereby provide a uniform environment for CA curing within the cementitious matrix. The raised temperature would also have caused an increase the hydration rate during the heating period, since it is known that this rate increases with the temperature of the curing environment [58].

3. EXPERIMENTAL PROGRAMME

3.1 Summary of tests

The present experimental programme comprised two groups of tests; (i) flexural tests on unreinforced notched prismatic beam specimens of size 75x75x255mm; and (ii) direct tension tests on unreinforced notched 100mm cube specimens. Multiple tests series were undertaken in each of these groups, each of which had a different set of test parameters, as summarised in Table 4. In addition to the tests shown in Table 4, three control specimens (specimens with empty channels), three (100mm) cubes and three (100-200mm) cylinders were cast and tested for each concrete batch.

All specimens were loaded under displacement control using feedback from the crack mouth opening displacement clip gauge (CMOD CG) (See Figs 3 to 5). In addition, the vertical displacements for all beam tests were recorded using an LVDT mounted on an aluminium angle bracket (See Fig. 3). An LVDT was also mounted on the DT specimens, as shown in Figs. 5a and b.

The same agent supply procedure was used for all specimens that contained CA healing-agent, which allowed the CA to be supplied at either atmospheric or at an elevated pressure. The latter was supplied using a pressurised airline and a pressure regulator (SMC IR3000 - 03BG - R).

The steel moulds and 4mm diameter removable PET tubes used to form the flow channels are shown for the beam and DT cube specimens in Figs. 2a and 2b respectively. The u-shaped profile required for the DT tests (see also Figure 5) was formed by threading a 1mm diameter welding rod through each PET tube and then bending it to the required shape. It was found that the PET tubes could be pulled out by hand with relatively little effort when the specimens were demoulded, one day after casting. 6mm diameter PET healing-agent supply tubes were added to each specimen after casting, as illustrated in Figs. 3 and 5.

In two of the test series (SF1-SF3 and DT1-DT2), the primary cracks were held stationary for a fixed healing period. In these tests, the healing-agent supply was not activated until the start of the healing period and was stopped at the end of the healing period. By contrast, in the tests with continuously varying crack opening displacements (SO1-SO3 and SP1-SP3), the healing-agent supply was activated at the start of each test and maintained until the end of each test.

Table 4. Summary of experiments

Group	Series and set	Description	No. of SH specimens per set	Size of specimens (mm)	CMOD/ LVDT rate (mm/s)	CA supply Pressure (bar)	Healing period (secs)	CMOD during healing (mm)	Max CMOD (mm)
1	SF1 SF2 SF3	Fixed crack healing period tests on notched specimens under 3-point loading	12	75x75x255	Gradual (0.0002 to 0.001)	0[1]	120 300 600	0.15	0.5
	SO1 SO2 SO3 SO4	Variable crack opening rate tests on notched specimens under 3-point bending	12	75x75x255	0.0002 0.0005 0.001 0.002	0.5	Variable	Variable	0.3
	SP1 SP2 SP3 SP4	Variable CA pressure on notched specimens under 3-point loading	12	75x75x255	0.001	0 0.1 0.3 0.5	Variable	Variable	0.3
2	DT1_1 DT1_2 DT1_3	Direct tension tests on notched cube specimens with fixed healing periods	18	100x100x100	0.0001	0.5	0 300 600	0.1 0.1 0.1	0.2
	DT2_1 DT2_2 DT2_3						0 300 1200	0.2 0.2 0.2	0.3

[1] No external pressure was applied to the healing-agent in these tests but an initial (relatively low) pressure (above atmospheric) was created by the head of CA in the supply tubes, which was approximately 200mm.

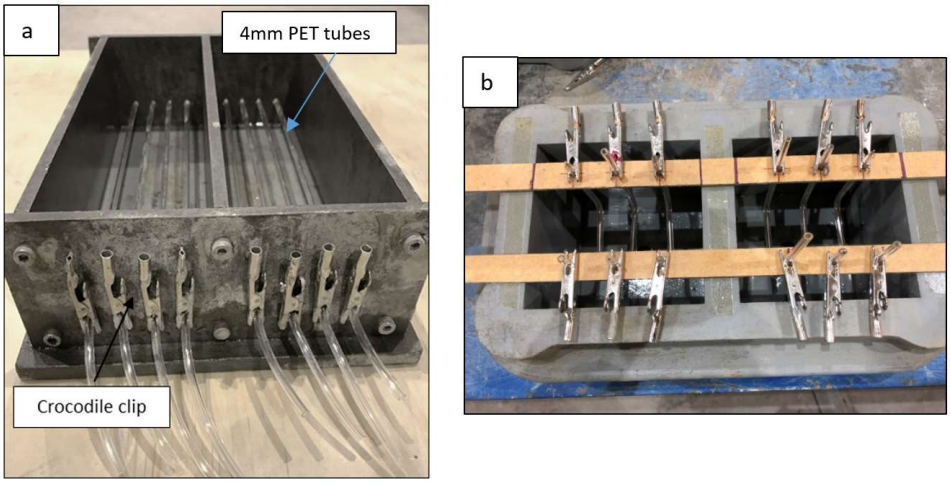

Fig. 2. Moulds for (a) beam and (b) direct-tension test cube specimens, showing PET tubes used to form flow channels

3.2 Group 1. Flexural tests on notched prismatic concrete beams

The aim of the Group 1 test series was to explore the interaction between cracking and healing under different loading and healing-agent supply scenarios. The test setup used for the experiments in this group is illustrated in Figs. 3 and 4 and details of each series are supplied below.

The fixed crack healing period (SF1-SF3) tests measured the degree of healing in specimens that contained a single stationary macro-crack. Each of these flexural cracks was formed before the healing-agent was released and then the beams were held at a fixed crack opening displacement for a selected period of time (see Table 4) prior to being loaded to failure. The same supply pressure and fixed crack opening displacement was used for all three test sets in this series.

The varying crack opening rate (SO1-SO4) test series measured the response of the notched prismatic beams to continuous loading. In these tests the rate of loading was controlled so that a constant crack mouth opening displacement (CMOD) rate was maintained. After some trial tests, a range of rates was selected that ensured that the cracking and healing processes overlapped (see Table 4). The same supply pressure was used for all of these tests.

The varying CA supply pressure test series (SP1-SP4) aimed to find the optimum delivery pressure for the current system. The specimens in this series were all loaded at the same constant CMOD rate, but the supply pressure was varied between the test sets from 0 to 1 bar (see Table 4 for the exact values).

The results of all Group 1 tests are presented in Section 5.1.

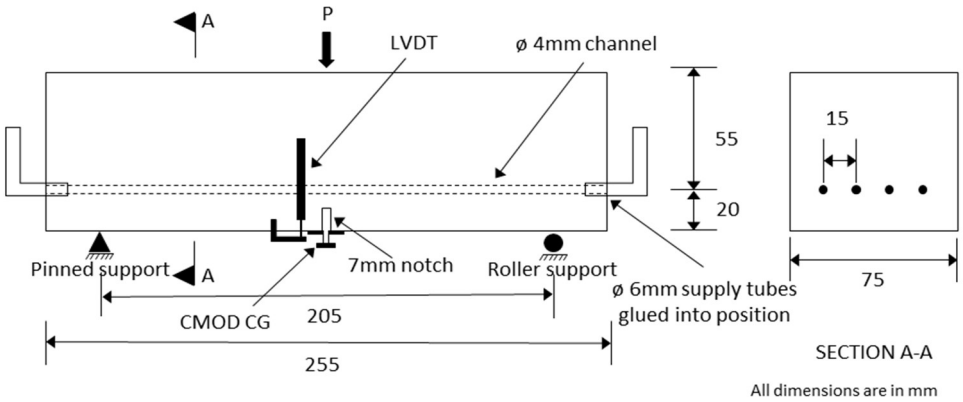

Fig. 3. General arrangement of beam specimens

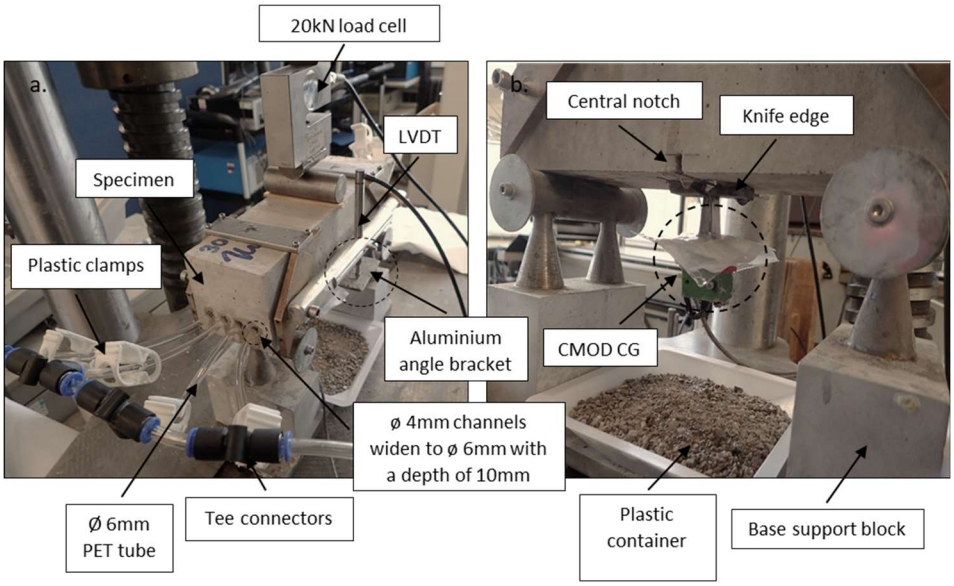

Fig. 4. Annotated photographs of the beam specimens in the testing rig

3.3 Group 2. Direct tension tests using 100mm notched cube specimens

The direct tension tests (DT1-DT2) were undertaken to find out if the characteristic healing behaviour exhibited in the tapering beam cracks would be replicated in a horizontal crack of (nominally) uniform opening. A further aim of the DT test series was to measure how the healing response changed with the crack opening displacement.

The difficultly of achieving consistent results from direct tension tests that capture stable softening behaviour has been discussed by a number of authors [59-61]. This difficulty is compounded when a static healing phase is introduced into the test [45]. The present authors undertook many trials, as explained in Selvarajoo [62], before a consistent set of test data was obtained for self-healing specimens loaded in direct tension.

The shape of the specimens, depth of the notches and the testing procedure used for this test series were guided by the work of Jacobsen et al. [61]. The cube shaped specimen with deep notches was preferred over a dog-bone shaped specimen because the former provided certainty on where the macro-crack would occur and ensured that a single macro-crack formed across each specimen. This meant that the LVDT and clip gauge would always capture the crack opening displacement and this set-up also guaranteed that healing agent was delivered to a single primary crack in a known location.

As noted by previous investigators [59-61], it is important to use a relatively stiff testing rig. The specimens were bonded to the pre-mounted 50mm thick steel loading plates with a two-part epoxy adhesive. To facilitate the formation of a good bond, a compressive force of 0.25kN was applied to the specimen immediately after the glue had been applied to the surfaces and the specimen had been placed in the rig. This load was maintained for a period of approximately 6 hours.

The overall experimental arrangement is illustrated in Fig. 5, which shows that three channels were used to deliver healing-agent to the crack. Two crack openings were used, and three fixed healing periods were considered (see Table 4). The same supply pressure was used for all experiments.

The results of the Group 2 tests are presented in Section 5.2.

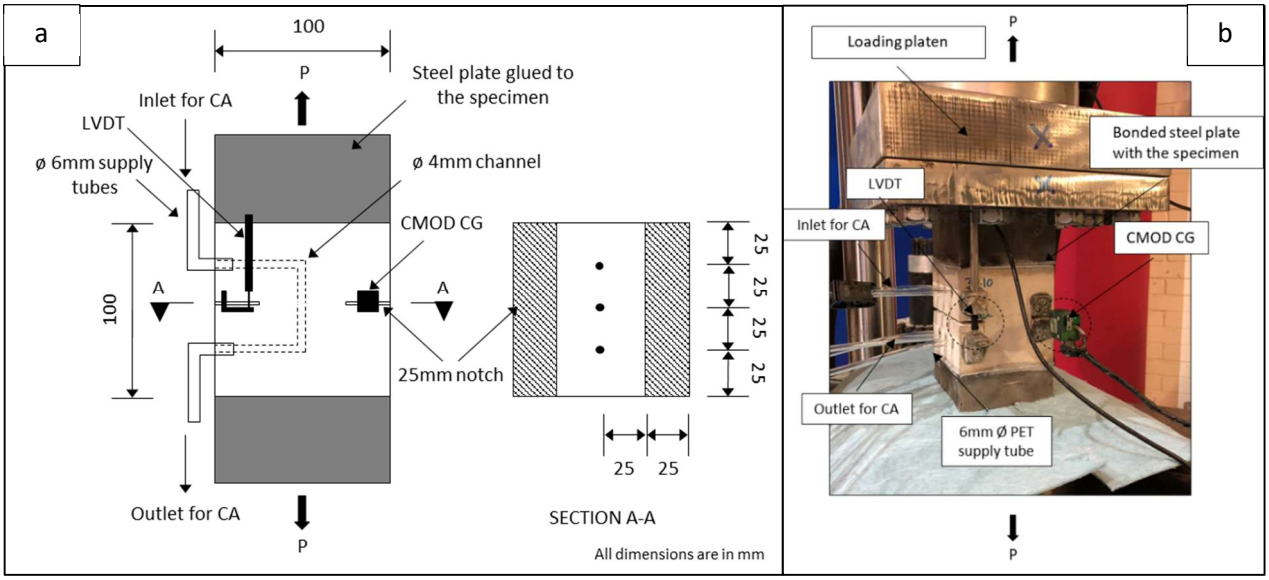

Fig. 5. Direct tension tests: (a) schematic of testing arrangement and (b) photo of a specimen in the testing rig

4. DAMAGE-HEALING MODEL AND HEALING INDICES

4.1 Damage-healing model

When considering the findings from experiments on self-healing cementitious materials, it is useful to be able to interpret the results in the light of a constitutive damage-healing model. A number of such models were discussed in [3] (e.g. [63-65]) and a general form of damage-healing model was suggested. When

applied to the normal response of a 'crack-plane', or cohesive zone [66], this model may be represented by equation (1).

The term 'damage' is used because the model was developed from damage mechanics principles [3]. In general, cracking is only one possible type of damage but in this paper the term damage is only associated with macro and micro cracking. A 'crack-plane' [67] is defined as the mid-surface of a narrow band of material that contains a macro-crack or a number of micro-cracks. The width of the band is equated to the thickness (w_b) of the fracture process zone [68], which may be taken as 3 times the size of the maximum aggregate size, when applied to concrete or mortar. The area of the crack-plane is assumed to be sufficiently large to represent the characteristic behaviour of the cementitious material under consideration. The elastic normal stiffness of this band (K) is then equal to E/w_b, where E denotes Young's modulus.

In this model, the mean stress across the crack-plane comprises two components, which are represented by the two terms on the right-hand-side of equation 1. The first component is associated with the undamaged (or virgin) material (v). The second component accounts for the stress transferred across the healed component of material (h), which may re-damage. The relationship is cast in terms of the relative normal displacement across the crack-band (u) and the normal stress component (σ), as follows;

$$\sigma = \sigma_v + \sigma_h = (1-\omega)\,\sigma_{ve} \;+\; \omega\, h_\omega (1-\omega_h)\sigma_{he}$$
$$= (1-\omega)\,K\,u \;+\; \omega\, h_\omega (1-\omega_h)\,K\,(u-u_h) \qquad (1)$$

in which, ω is the scalar damage variable, which lies in the range 0 (no damage) to 1 (fully damaged); h_ω represents the portion of damaged material that has been healed; u_h denotes a 'healing' relative-displacement, which is the crack opening displacement at the time healing takes place; ω_h is the scalar re-damage variable; and σ_{ve} and σ_{he} are the stresses on the undamaged parts of the virgin and healed components of material respectively.

The inelastic components of u and (u- u_h) are denoted u_{dam} and u_{redam} respectively, which are given by the following relationships;

$$u_{dam} = u - u_{el} \qquad (2a) \qquad \text{and} \qquad u_{redam} = u - u_h - u_{el} \qquad (2b)$$

in which $u_{el} = \sigma / K$

The damage evolution functions (equations 3a and 3b), that define ω and ω_h, depend on the maximum values of the inelastic relative displacements, which are denoted by damage parameters ζ and ζ_h respectively.

$$\omega(\zeta) = 1 - \frac{f_t}{K\cdot\zeta} e^{\frac{-c_1\zeta}{\zeta_m}} \qquad (3a) \qquad \text{and} \qquad \omega_h(\zeta_h) = 1 - \frac{f_{th}}{K\cdot\zeta_h} e^{\frac{-c_1\zeta_h}{\zeta_{mh}}} \qquad (3b)$$

in which f_t is the tensile strength; ζ_m is the relative-displacement at the effective end of the softening curve [67] and c_1 (=5) is a softening constant.

The softening function was originally derived from a strength decay function (ϕ) [69] such that;

$$\sigma = f_t\,\phi = (1-\omega)\,K\,u \qquad \text{for } u \geq u_t \qquad (4)$$

which, noting that u_t is defined by $u_t = \frac{f_t}{K}$, leads to;

$$\phi(\zeta) = \big(1-\omega(\zeta)\big)\frac{u}{u_t} \qquad (5)$$

Here, the effective end of the fracture damage evolution functions (3a and 3b) are defined in terms of ζ_m and ζ_{mh} but these may alternatively be expressed in terms of the virgin and healed fracture energies parameters, G_f and G_{fh} respectively, which are defined by;

$$G_f = \int_0^\infty \sigma_v \,\mathrm{d}\zeta \qquad (6a) \qquad \text{and} \qquad G_{fh} = \int_0^\infty \sigma_h \,\mathrm{d}\zeta_h \qquad (6b)$$

The authors considered that there was value in generalising equation (1) to a notched beam situation in an empirical manner. A justification for this equation and the dependent functions are given in Appendix A. The phenomenological equation proposed is as follows;

$$P = \left(1 - \omega_\psi\right) K_\psi \, u_\psi \; + \; \omega_\psi \, h_{\omega\psi}\left(1 - \omega_{h\psi}\right) K_\psi \left(u_\psi - u_{h\psi}\right) \tag{7}$$

in which P is the central point load on a beam loaded in three-point bending (see Fig. 3); u_ψ is a representative displacement (i.e. central deflection or crack mouth opening displacement); K_ψ is the initial linear slope of the P v u_ψ curve, and is determined from the experimental response; the damage and healing variables, with subscript ψ, are the generalised scalar variables that relate to the specific beam test under consideration.

4.2 Relationship between healing indices and the healing parameters

Homma et al. [70] proposed a healing index of the form shown in equation (8) and this healing (or recovery) index has also been adopted by other investigators [44,71];

$$H_\sigma = \frac{\sigma_3 - \sigma_2}{\sigma_1 - \sigma_2} \tag{8}$$

in which the average uniaxial stress terms (σ_i) are defined in Fig. 6 and it is noted that $\sigma_1 = f_t$.

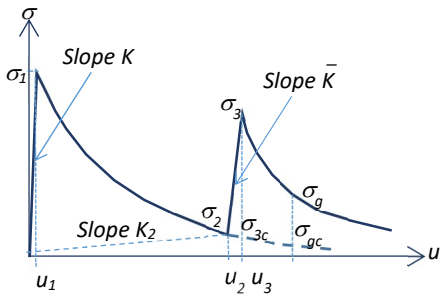

Fig. 6. Typical damage-healing-redamage response in uniaxial tension

Assuming that damage continues in the virgin part of the material during the reloading phase (i.e. from points 2 to 3), a more logical definition of H_σ would use σ_{3c} in place of σ_2 in equation (8). The challenge of this approach is that a control curve is needed that is fully consistent with the damage-healing curve. Control curves are available for all of the test series undertaken in the present study, but due to the statistical variation of concrete these will always depart from the theoretical control curve associated with the test under consideration. Since the amount of virgin damage that occurs between points 2 and 3 on the graph is usually negligible, the definition given in equation (8) will be adopted for tests with fixed-crack healing periods. However, when considering processes in which damage and healing occur simultaneously, this assumption is no longer reasonable and therefore equation (9) will be used for these cases. It is acknowledged that indices computed from equation (9) are affected by the aforementioned statistical variation in behaviour;

$$H_\sigma = \frac{\sigma_g - \sigma_{gc}}{\sigma_1 - \sigma_{gc}} \tag{9}$$

in which σ_g and σ_{gc} are defined in Fig. 6

The indices defined in equations (8) and (9) relate to strength recovery but a stiffness recovery index is also defined as follows;

$$H_K = \frac{\bar{K} - K_2}{K - K_2} \tag{10}$$

in which K is the initial (pre-cracked) slope of the response curve and $\bar{K}$ represents the slope from points 2 to 3, as illustrated in Fig. 6

The question then arises of how these healing indices relate to the healing parameter (h_ω). Considering first the stiffness index; using the theoretical terms from equation (1) in equation (10) leads to the following expression for H_K;

$$H_K = \frac{\left((1-\omega_2)K+\omega_2\, h_\omega\, \mathrm{K}\right)-(1-\omega_2)K}{K-(1-\omega_2)K} = h_\omega \tag{11}$$

It may be seen that the stiffness healing index defined in (10) is consistent with the healing parameter (h_ω).

Undertaking the same process for the strength healing index, gives the following;

$$H_\sigma = \frac{(\phi_2 f_t+\omega_2 h_\omega K\Delta u)-\phi_2 f_t}{f_t-\phi_2 f_t} = \frac{\omega_2}{(1-\phi_2)}\frac{f_{th}}{f_t}h_\omega \tag{12}$$

in which $\Delta u = u_3 - u_2$ and the strength of the healed material is related to the change of stress in the healed proportion of material in the reloading step i.e. $f_{th} = K\Delta u$.

When a fully healed crack has the same strength as the virgin material and the crack is fully formed at the time of healing (i.e. ω = 1 and ϕ = 0), then H_σ would be equal to h_ω.

Some authors report filling indices [72], which provide a measure of the relative area of a crack that is filled with healing agent. This is straight forward to determine from experimental observations when the crack is filled with healing products that are weaker than the parent material and when re-cracking occurs in the same plane as the original crack. It is much more difficult to determine when the healed zone is stronger than the original material. In the latter case, re-cracking tends to occur in a different location from the first crack [6]. However, if it is assumed that the re-cracked material has the same average strength as the virgin material and all of the agent that fills a crack cures fully, then H_σ has the same value as the filling index.

5. RESULTS

This section now presents the results from the two groups of tests.

5.1. Group 1 tests on beam specimens with fixed healing periods (SF1-SF3); varying crack opening rates (S01-S04) and varying CA supply pressures (SP1-SP4).

The load v CMOD and load v LVDT responses of a typical control specimen are shown in Figs. 7a and 7b respectively. The specimen exhibits the classical post-peak softening response of a notched plain concrete specimen [73]. The characteristics of the load-CMOD and load-LVDT responses are very similar and thus from this point onwards, only load-CMOD responses will be shown in this paper for the Group 1 beam tests; however, all of the data gathered are presented in the PhD thesis of Selvarajoo [62] and are available at M4L [74].

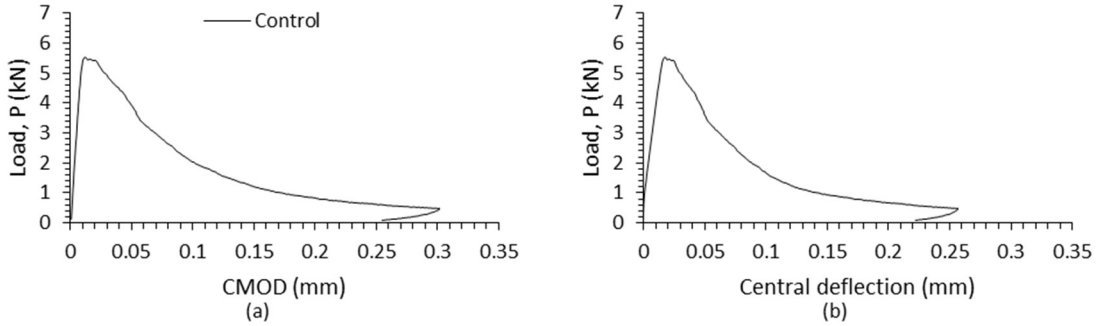

Fig. 7. (a) Load v CMOD and (b) load v central deflection responses for control specimens at a CMOD rate of 0.0005mm/s

5.1.1 Tests on beam specimens with fixed healing periods (SF1-SF3)

Fixed healing period beam tests were conducted with healing periods from 2 to 60 minutes, but the results changed by an indistinguishable amount after 5 minutes and so here only the 2, 5 and 10 minutes healing period results are presented. The load v CMOD responses, given in Figs. 8a-c, show that the post-healed

peak load exceeded the pre-healed peak load in all cases. The results showed a modest increase of healing index from 2 to 5 minutes although the responses suggest that healing was substantially complete (~88%) within the first two minutes.

Each graph also includes the results from a numerical computation undertaken with the model described in Section 4 and Appendix A. The model was calibrated to the experimental responses, but the same parameters were used for all simulations except the degree of healing parameter (h_ψ), which was assumed to vary with healing time. The calibrated parameters are given in Table 5. The strength decay parameters used were $c_1=5$, $m=14$, $a_t=0.5$, $m_h=18$ and $a_{th}=0.5$.

Table 5. Model parameters

Series / healing time	CMOD at healing mm	P_t (kN)	P_{th} (kN)	K_ψ (kN/mm)	$u_{m\psi}$ (mm)	$u_{mh\psi}$ (mm)	H_K, h_ψ	H_σ	G_{fv} N/mm	G_{fh} N/mm
SF1 / 120s							0.875	1.02	0.107	0.094
SF2 / 300s	0.15	6	6	666.67	0.45	0.45	0.9	1.05		
SF3 / 600s							0.925	1.08		

A clear trend in all of the test results is that the post-healed softening branch of the load-CMOD curves is steeper than the corresponding pre-healed response, which is consistent with the fracture energy of the healed material being lower than that for virgin material (see Table 5). The model predictions suggest that the effective degree of healing was between 0.875 and 0.925. An attempt was made to confirm these proportional healing figures with visual observations, but the re-cracked areas were difficult to measure because, as explained below, re-cracking generally occurred in a different location from the first crack. Also, in some areas, a reaction between CA and the cementitious compounds resulted in brown deposits on the crack surface, as may be seen in Figure 13, but in other areas, clear cured CA was visible on the crack surface after the test; however, the latter is difficult to distinguish from a photograph. It was concluded that the most reliable way to determine the effective degree of healing for the current healing system was from the response curves.

The tensile strength of cured CA is quoted as being 21MPa, which is considerably stronger than the tensile strength of the concrete (3.4MPa) (see Section 2.2). This implies that a specimen will not re-crack directly through the cured healing-agent but rather will re-crack adjacent to the healed zone. However, as pointed out by Joseph et al. [6], this interface zone isn't formed only of plain concrete, since the CA permeates into the microcracked zone adjacent to the macro crack (see Fig. 9), cures and creates a cementitious-polymer composite with a higher strength than the original material.

A secondary trend is evident, which is that the load reduces noticeably during the fixed crack opening healing period and then that the CMOD readings initially reverse when loading restarts. This response may be associated with short-term creep and/or the effects of the pressurised healing-agent flowing into the crack.

The CMOD provides a measure of the crack opening near the lower surface of the specimen. When full (or near full) healing occurs, the post-healed crack width is relative to the crack-opening at healing. Thus, for the present case, which had a crack opening of 0.15mm during the healing period and a final CMOD of 0.4mm, the near surface crack opening at the end of these healing tests would have been 0.25mm.

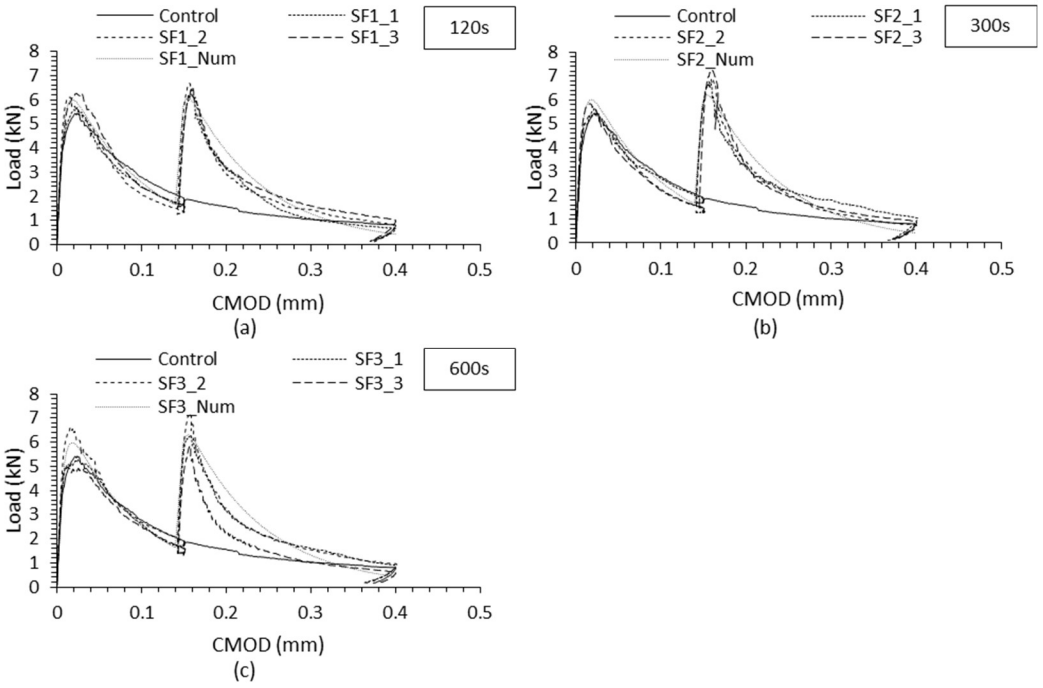

Fig. 8. Load v CMOD responses for different healing periods: (a) 120 seconds, (b) 300 seconds and (c) 600 seconds

Fig. 9. Photo of an SF test specimen showing the primary crack and CA on the surface

5.1.2 Test with different varying crack opening rates (SO1-SO4)

Results from the tests with different CMOD rates are presented as load v CMOD and healing index v CMOD responses in Figs. 11a-d and 12a-d respectively. In addition, a comparison of control specimen responses with different CMOD rates is presented in Fig. 10. By comparing the results of the healing tests with those of the corresponding control specimens, it is clear that significant healing occurred in all cases. However, the responses are very different from those of the fixed healing (SF) tests (Figs 8a-c) in three ways; (i) the post-healed peak loads are significantly lower than those of the SF tests; (ii) the post-healed responses exhibit lower average rates of softening; and (iii) the post-healed responses exhibit multiple peaks (for nearly all specimens). It is believed that these SH responses indicate that multiple healing-damage events occurred, and that damage and healing progressed simultaneously.

The graphs in Fig. 11a-d show considerable variability both within the test sets and between sets, and it is noticeable that the responses become smoother as the CMOD rate increases. This latter trend is attributed to the fact that, as the CMOD rate increases, so does the rate at which healed material is restressed. Therefore, each component (or elemental area) of healed material reaches the re-damage threshold more quickly and the relative area of healed material that has reached this threshold is less. This results in smaller ‘jumps’ in the response due to re-healing and re-damage.

Healing is judged relative to the associated control specimen, but it is known that the rate of loading affects the fracture softening response of plain concrete [73], with the post-peak response being apparently more ductile and the peak strength increasing with loading rate. This trend is exhibited in the present data. Since healing indices are computed relative to the associated control tests (i.e. those with matching CMOD rates), these indices are rate appropriate and can be used to validate a rate dependent healing model. It is noted

that the fracture rate effect for plain concrete can be readily taken into account in a fracture model, as described in reference [73].

The CMOD value at which the response of the healed specimens starts to depart significantly from that of the control specimen varies between the different tests. There is no clear pattern to this behaviour but it is apparent that the crack needs to reach a certain threshold before the CA is transported into the crack and that there is a lag in time from when the agent first flows into the crack to the point at which appreciable healing begins. It is estimated that the threshold CMOD for CA transport is between 0.03mm and 0.05mm.

In addition, there is a tendency for CA 'pipes' to form in supply channels. Evidence from the tests suggests that the thickness of the pipe walls remains negligible during the tests, but if a specimen is left for a number of days, the formation of this CA 'pipes' becomes clear, as illustrated in Fig. 13.

Unlike the fixed healing period tests, there is no clear definition of the clear crack opening in the present continuous tests in which re-healing and re-cracking occur simultaneously. The fact that healing continues until the end of these tests suggests that there are areas in which healed material bridges between the crack faces.

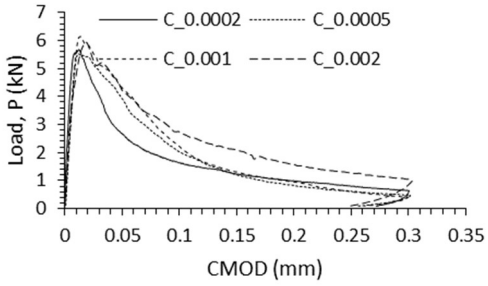

Fig. 10. Response of beam control specimens at different CMOD rates (mm/s)

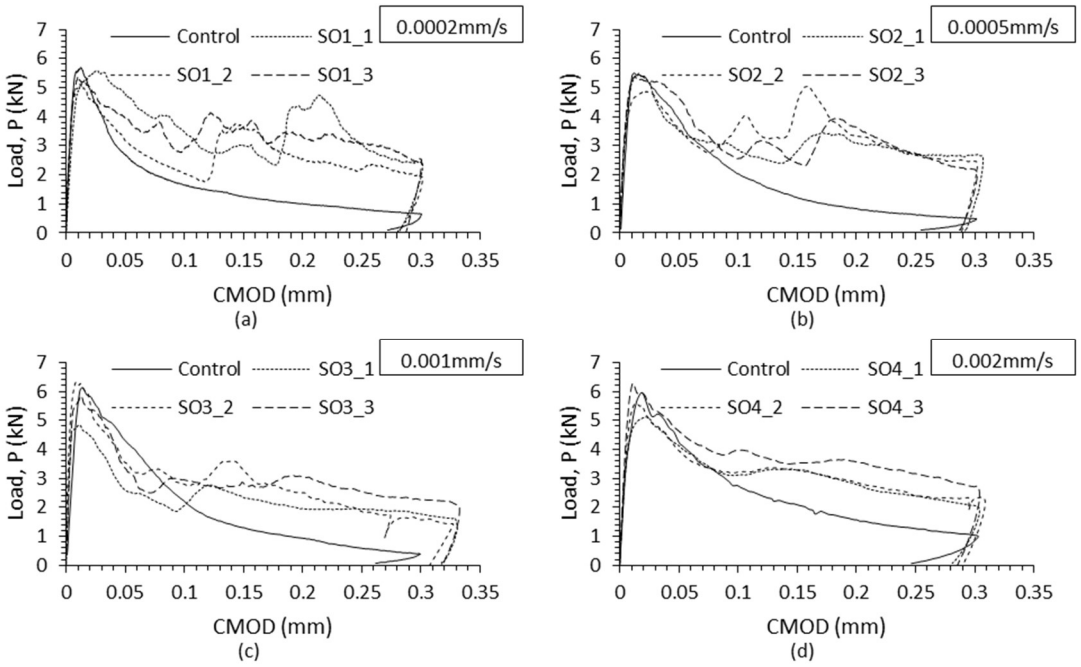

Fig. 11. Load v CMOD responses at CMOD rates of (a) 0.0002mm/s (b) 0.0005mm/s (c) 0.001mm/s and (d) 0.002mm/s

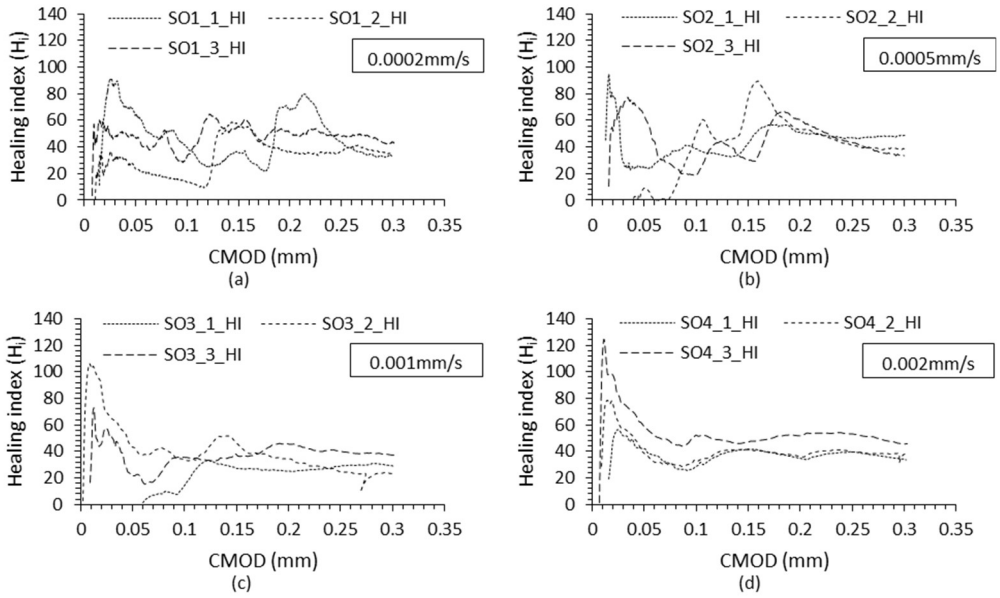

Fig. 12. SO series healing indices at CMOD rates of (a) 0.0002mm/s, (b) 0.0005mm/s, (c) 0.001mm/s and (d) 0.002mm/s

Fig. 13. The formation of CA 'pipe' (circled)

5.1.3 Tests with varying CA supply pressures (SP1-SP4).

The load v CMOD responses from the tests with different supply pressures are shown in Fig. 14a-d. From these graphs it is apparent that least healing was observed in the tests that relied solely on capillary tension to transport the healing-agent into the crack (i.e. the 0-bar case) and the greatest healing in the specimens for which the supply pressure was 0.3 bar. At higher pressures, there was a tendency for the CA to flow out of the sides of the crack, which implies that the body of healing fluid in the crack was in flux and therefore less likely to cure. From these tests, it would appear that the optimum supply pressure lies between 0.3 and 0.5 bar. The authors believe that in a more constrained situation (e.g. in a cracked specimen with sealed surfaces), maximum healing would be exhibited at a higher delivery pressure, since the flux level within the body of healing agent would be reduced.

Another notable characteristic in these test data is that the CMOD (and time) at which measurable healing commences reduces as the delivery pressure increases (see Fig. 15a-d). This is believed to be because pressurised liquid will flow through a smaller opening (crack) than unpressurised liquid.

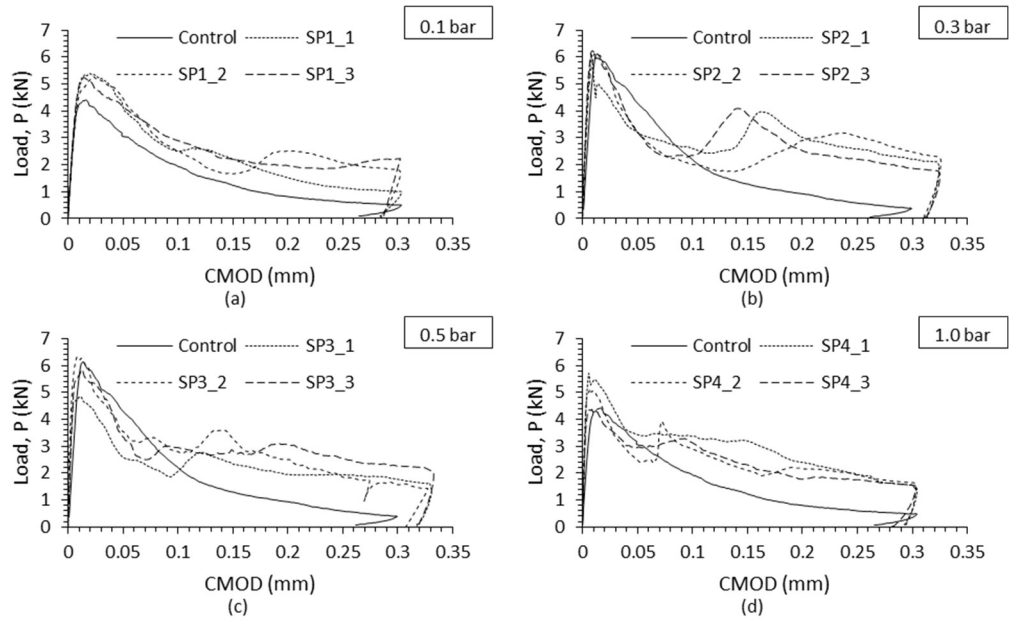

Fig. 14. Load v CMOD responses at CA supply pressures of (a) 0 bar, (b) 0.3 bar, (c) 0.5 bar and (d) 1.0 bar

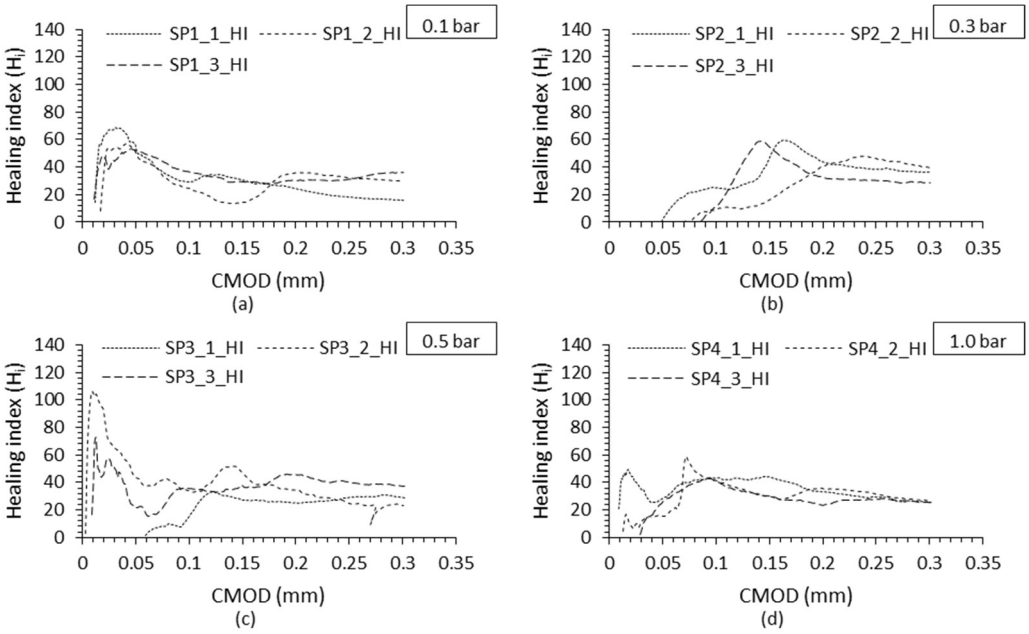

Fig. 15. SP series healing recoveries at pressures of (a) 0 bar, (b) 0.1 bar, (c) 0.3 bar, (d) 0.5 bar and (e) 1.0 bar

5.2 Group 2 tests (Series DT1 and DT2)

Attention is now turned to the results of the direct tension tests.

The upper platen of the loading rig (see Fig. 5b) has the freedom to rotate and in some tests CMOD and LVDT readings became different from one another, which indicates appreciable rotation of the upper platen. For this reason, both LVDT and CMOD results are presented for the direct tension tests.

The deep notches result in the formation of a single primary crack, as illustrated in Fig. 16. However, the softening response is strongly affected by how the cracks from the notches on opposing faces propagate and join. If there is a significant offset (e.g. 20mm) between the propagation lines of the opposing cracks, there tends to be a step in the load-displacement response when the cracks come together. By contrast, when the cracks from the two edges are closely aligned, the response tends to be smoother. In some test responses there is an unloading-reloading cycle in the softening phase, which occurs when the rate of crack formation

exceeds the response rate of the feedback loop; however, such cycles are not considered to invalidate the test provided that the softening branch is regained. The contrasting responses are illustrated in Fig. 17, which shows results from three different control tests, each of which exhibit one of the aforementioned characteristics (i.e. smooth (C1) response, response with a step (C2) and an unloading-reloading cycle (C3)).

Fig. 16. Final crack pattern of a DT control specimen

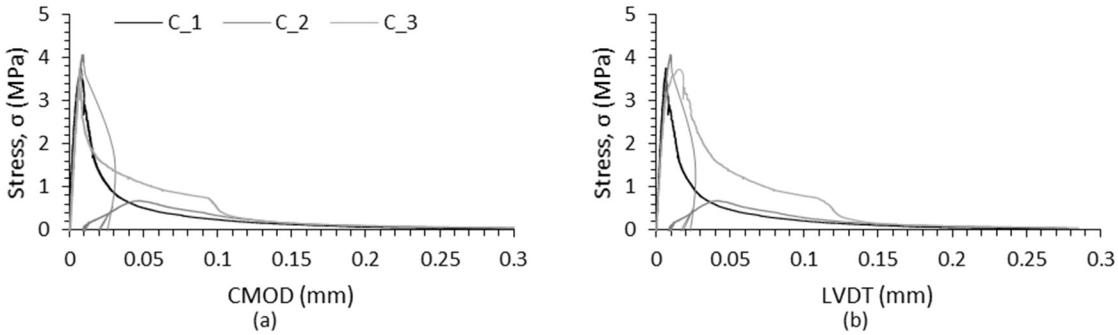

Fig. 17. Load v CMOD and load v LVDT responses for the control specimens showing C1, a smooth response, C2, a response with a step and C3, an unloading-reloading cycle.

The responses from the DT series of tests, which had healing CMODs of 0.1mm (DT1 to 3) and 0.2mm (DT4 to 6) respectively, are presented in Figs. 18a-f and 19a-f respectively. The stress (σ) is defined as the load (P) divided by the ligament area (5000mm^2) and is plotted as a function of CMOD (mm) and LVDT (mm). The fixed healing periods for each test set varied from 0 to 600s for DT1 to 3 and 0s to 1200s for DT4 to 6. The DT6 set of tests, with a healing period of 1200s, was undertaken after the other tests because it was apparent that the healing-agent had not fully cured in 600s tests with a crack opening of 0.2mm. In the tests labelled '0s' (i.e. DT1 and DT4), loading was paused when the requisite CMOD had been reached but restarted as soon as the CA had flowed into the specimen and the meniscus in the delivery tubes had stabilised, which took between 7 to 10s. Also, it is estimated that some CA reached the crack less than 1s from the release time. Thus, the '0s' test should be considered more like a 10s test, albeit that the quantity of CA in the crack would have been variable in this period.

Results from numerical simulations using the constitutive model described in Section 4 are also presented on the graphs. The calibrated parameters used for each simulation are shown in Table 6. As for the beam model simulations, the parameters were fixed for all test sets except for the healing parameter h_ω, which was assumed to varying with the healing period.

Table 6. Model and computed parameters

Series / healing time	CMOD at healing (mm)	f_t (N/mm^2)	f_{th} (N/mm^2)	K (N/mm^3)	u_m (mm)	u_{mh} (mm)	H_σ	h_ω, H_K	G_{fv} (N/mm)	G_{fh} (N/mm)
DT1/0s DT2/60s DT3/300s	0.1	3.75	3.75	535.71	0.2	0.4	0.46 0.47 0.48	0.43 0.44 0.45	0.176	0.326
DT4/0s DT5/60s DT6/1200 s	0.2	3.75	3.75	535.71	0.2	0.4	0.2 0.21 0.27	0.2 0.21 0.27	0.176	0.326

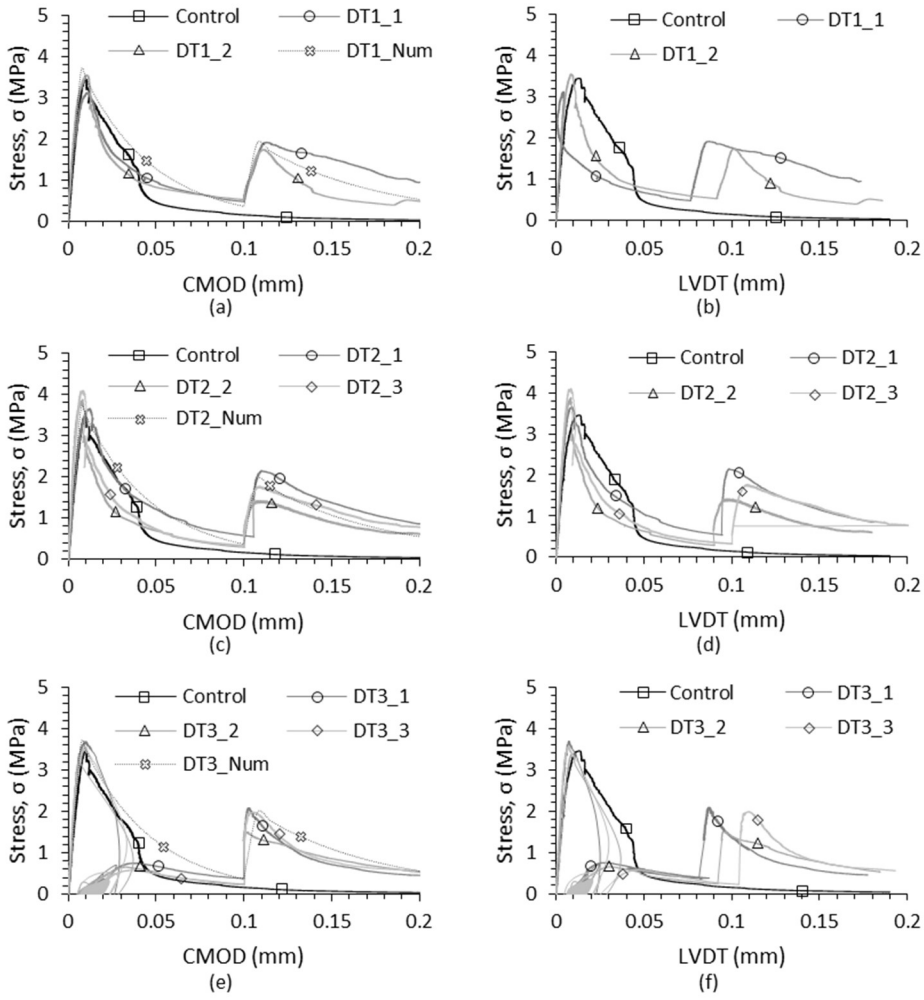

Fig. 18. Load v CMOD and load v LVDT responses of DT specimens with 0.1mm crack opening for healing periods of (a-b) 0 seconds, (c-d) 60 seconds and (e-f) 600 seconds

Comparing the results of the 0.1mm tests (DT1-3) with the 0.2mm tests (DT4-6), shows that significantly more healing occurred in the former. This is evident from the increase in respective healing indices as well as from the associated healing parameter values in Table 6.

In both test series, the initial slope of the reloading response curves (i.e. the response immediately following the healing period) increases with the length of the healing period. However, there is not a corresponding increase in the peak post-healing loads. Also, these reloading response curves show a greater degree of nonlinearity when the healing period is shorter. Only the final set of tests in each series (i.e. DT3 and DT6) had responses close to those of the numerical model. The apparently more ductile response of the tests with shorter healing periods is assumed to indicate that in these tests (i.e. DT1-2 and DT4-5) a significant

proportion of the healing-agent was only partially cured, and that re-healing and re-damage processes were happening simultaneously during the final loading stage.

The fact that the peak post-healed loads did not increase in the same proportion to the reloading stiffness suggests that the proportion of the crack that is healed by fully cured agent is lower than the total area affected by the healing-agent. This leads to the conclusion that in some areas of the crack the CA did not stabilise and cure. This trend increases as the crack opening increases.

Visual observations during and after the tests show that re-cracking, after healing, occurred in a slightly different location from the primary crack, as illustrated in Fig. 20a. This is consistent with the findings of Joseph et al. [6].

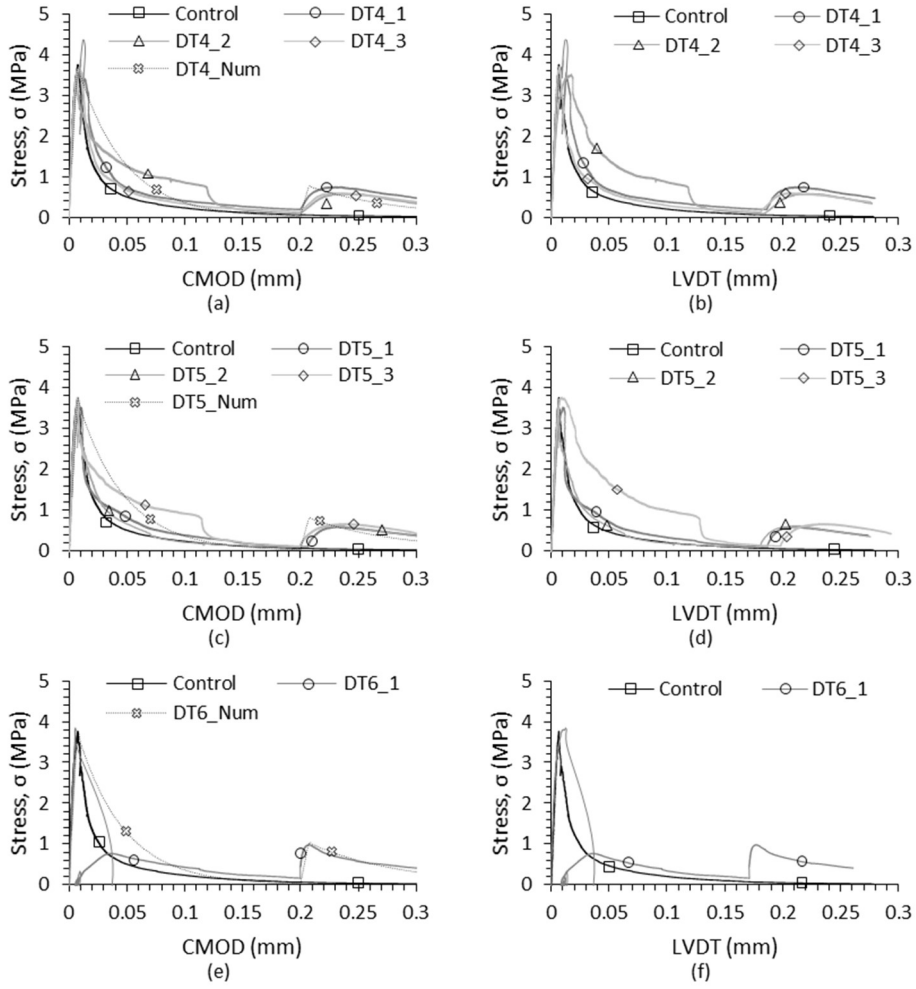

Fig. 19. Load v CMOD and load v LVDT responses of DT specimens with 0.2mm crack opening for healing periods of (a-b) 0 second (c-d) 60 seconds and (e-f) 1200 seconds

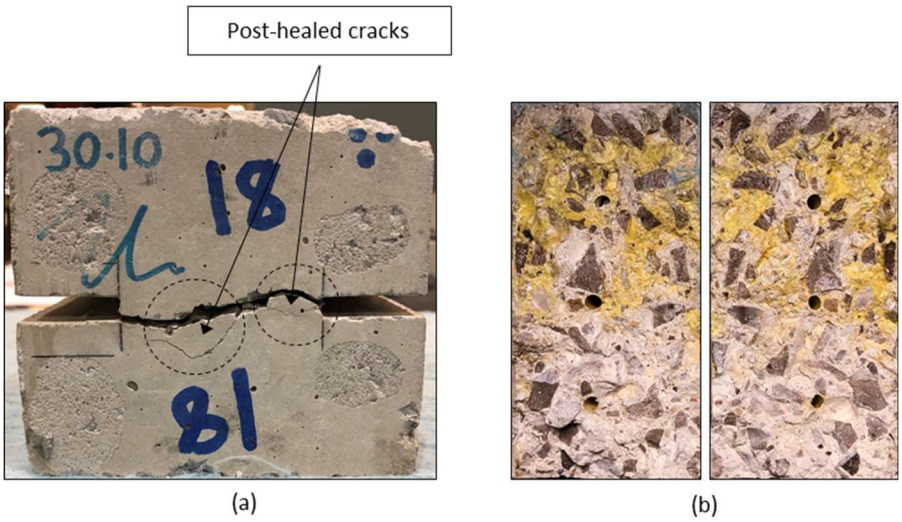

Fig. 20. (a) Final crack pattern of a representative SH specimen and (b) re-cracked surface after the test.

The degrees of healing in both sets of DT tests are significantly lower than those for the comparable notched beam tests, for which the CMOD was 0.15mm. In the notched beam tests, the macro-crack tapers from a maximum value at the crack mouth to zero at the crack tip, although the area around the nominal crack tip will comprise a network of micro-cracks [68].

Furthermore, the effectiveness of healing in the beams suggests that when healing-agent flows upwards into a tapering vertical crack from a set of delivery channels, the healing-agent stabilises and cures in a more effective way than when delivered via three channels into a horizontal uniform crack. In these particular (DT) tests, more healing occurred in the specimens with narrower cracks, although the authors would expect a more viscous agent to be effective in larger cracks. In general, this finding does not imply that autonomic systems are not effective at healing larger serviceability sized macro-cracks (e.g. 0.3-0.5mm), since the effectiveness of these systems for such cracks has already been proven in a number of studies (1,5,6,24).

The amount of healing-agent in the supply reservoir continued to decrease significantly during the healing phases, although the rate of reduction reduced over time. Some CA flowed out of the specimen, but a significant quantity also flowed into the micro-cracked region that surrounded the macro-crack. It is concluded that the viscosity of the CA was too low to achieve a stable body of adhesive across the entire crack surface for these crack openings and supply pressure. It also appears that the crack boundary conditions, and possibly the orientation of the crack, have a strong influence on the degree of healing.

The healed material fracture energies displayed in Table 6 are higher than those of the virgin material, which is in contrast to the trend found in the SF beam series. We think that this is because simultaneous damage and healing progressed in the final loading stages of the DT tests, whereas in the SF series, healing was negligible in the final loading stage. This implies that the response in the final loading stage of the DT tests was not governed solely by the re-damage response and thus the assumptions used to compute the G_{fh} values are not wholly valid.

6. CONCLUSIONS AND CLOSING REMARKS

6.1 Summary of findings and conclusions

New data has been presented on the response of concrete beam and direct tension specimens, with an embedded autonomic self-healing system, for a range of load paths. It has been shown that the behaviour of specimens subjected to a varying load (with a constant CMOD rate), in which cracking and healing occur simultaneously, is in marked contrast to that for a loading path that allows healing to take place under fixed crack conditions. The work has also confirmed the benefits of pressurising the healing agent and determined the optimum pressure range for a certain type and size of crack. Differences between the healing response in tapering beam cracks and uniform cracks in direct tension specimens have been revealed. The effects on

the damage-healing behaviour of varying the loading rate and of the crack opening displacement during fixed healing periods have also been quantified. The ability of the proposed damage-healing model to simulate the behaviour an autonomic self-healing material has been shown. Relationships between a set of mechanical healing indices and the healing parameter in a damage-healing model have been established. A number of specific conclusions have been drawn from this study, as follows:

i. A vascular system that uses embedded channels to deliver CA to damage zones in concrete gives significant healing (30 to 108%) in cracks up to 0.2mm in width, with the healing index exceeding 100% in beams with a CMOD of 0.15mm and full healing being achieved within 2 to 3 minutes:
ii. A healed specimen has the same characteristic fracture response as a plain concrete specimen although the post-healed fracture energy in fully healed cracks with CA is lower than that of virgin cracks:
iii. Simultaneous cracking and healing occur when specimens are loaded such that the CMOD rate lies between 0.0002 and 0.002 mm/s, with the irregularity of the load-CMOD response increasing as the CMOD rate reduces:
iv. Pressurising the healing-agent leads to greater penetration into a crack network and to more healing, with the optimum supply pressure for tapering cracks (with a CMOD of 0.15mm) being between 0.3 and 0.5 bar:
v. Whilst the viscosity and curing rate of CA allow combined healing-damage behaviour to be studied in short term tests, the low viscosity leads to a significant loss of healing-agent from macro-cracks, particularly from horizontal cracks with a nominally uniform opening of 0.2mm or greater:
vi. The proposed damage-healing model provides a realistic representation of the mechanical behaviour of the present SHCM system.

6.2 Closing remarks

The findings from the two groups of tests provide a substantial body of data on the behaviour of this self-healing material system, which should prove useful to those developing design or computational models for SH material systems.

There are also a number of findings that should prove helpful to researchers developing healing systems that use autonomic healing-agents; particularly those related to the benefits of pressurising the healing-agent, the pros and cons of using a low viscosity healing-agent, the challenges of undertaking direct tension tests and the nature of simultaneous damage-healing behaviour.

The healing-agent delivery system has been shown to be a viable means of transporting healing-agents to damage zones, but it is acknowledged that reproducing such networks in large-scale civil engineering structures would present a considerable challenge.

ACKNOWLEDGEMENTS

The authors gratefully acknowledge the funding from UK-EPSRC Grant No. EP/P02081X/1, Resilient Materials 4 Life, RM4L.

Information about the data underpinning the results presented here, including how to access them, can be found in the Cardiff University data catalogue at http://doi.org/10.17035/d.2019.0081928129.

The authors would also like to acknowledge the considerable help and expertise of Richard Thomas and Ian King without whom the laboratory work would not have been possible.

APPENDIX A. A generalised damage-healing model for the flexural behaviour of notched beam tests.

When considering notched beam fracture-healing tests, such as those described in Section 3.2 it is necessary to solve a boundary value problem in order to determine the response of the beam specimen. This may be accomplished using, for example, a finite element idealisation of the beam, with an equation of the type presented in equation (1) being used to govern the constitutive behaviour at an integration point in the model.

The authors considered that there was value in generalising equation (1) to a notched beam situation in an empirical manner. Whilst this leads to an inferior idealisation to one based on the solution of a boundary value problem, this phenomenological model does prove a useful aid in characterising and interpreting the behaviour of notched beam damage-healing tests. The phenomenological equation proposed is as follows;

$$P = \left(1 - \omega_\psi\right) \mathrm{K}_\psi \, \mathrm{u}_\psi \; + \; \omega_\psi \, \mathrm{h}_{\omega\psi}\left(1 - \omega_{h\psi}\right) K_\psi \left(u_\psi - u_{h\psi}\right) \qquad \text{(A1)}$$

in which P is the central point load on a beam loaded in three-point bending (see Fig. 3); u_ψ is a representative displacement (i.e. central deflection or crack mouth opening displacement); K_ψ is the initial linear slope of the P v u_ψ curve, and is determined from the experimental response; the damage and healing variables, with subscript ψ, are the generalised scalar variables that relate to the specific beam test under consideration.

The damage evolution equations for the generalised damage variables are a modified form of equations 3a&3b , based on a function given in reference [75], which allow for the fact that the functions represent the mean damage through the depth of the cracked (or damage) zone, and because the damage parameters now relate to the representative displacement variable u_ψ

$$\omega_\psi\left(\zeta_\psi\right) = 1 - \frac{P_t}{K_\psi \cdot \zeta_\psi}\phi_\psi \qquad \text{(A2a)} \qquad \text{and} \qquad \omega_{h\psi}\left(\zeta_{h\psi}\right) = 1 - \frac{P_{th}}{K_\psi \cdot \zeta_{h\psi}}\phi_{h\psi} \qquad \text{(A2b)}$$

in which P_t and P_{th} are the virgin and healed peak loads respectively and the generalised strength decay function is as follows;

$$\phi_\psi\left(\zeta_\psi\right) = \frac{a_t}{\beta - 1} \, \mathrm{e}^{-c_1 \frac{\zeta_\psi}{\zeta_{\psi m}}} \cdot \left(\beta - e^{-c_1 m \frac{\zeta_\psi}{\zeta_{\psi m}}}\right) \qquad \text{(A3)}$$

in which c_1, m and a_t are model parameters that are calibrated to the experimental data and β is derived from the boundary conditions of the function, as explained in reference [72], and is given by the following equation;

$$\beta = \frac{c_1 a_t (1+m) + \left(\frac{\zeta_{t\psi}}{\zeta_{m\psi}}\right)}{\left(\frac{\zeta_{t\psi}}{\zeta_{m\psi}}\right) + a_t c_1} \qquad \text{(A4)}$$

The values of the parameters will be given in the results sections.

The function $\phi_{h\psi}$ takes the same form as equation (A3) except that the variables and constants are the healed material counterparts of the virgin material values shown in (A3).

It is emphasised that this model is not intended to be predictive, it is simply introduced as a tool for aiding the interpretation of the notched beam results presented in this paper. A separate paper [50] describes a full coupled nonlinear finite element model for these material systems, which does not have the aforementioned restrictions.

APPENDIX B. Healing agent flow and curing properties

This appendix provides a summary of the healing-agent flow and curing parameters determined in this study and reported in linked paper [51].

Capillary flow parameters

The CA capillary flow parameters for the modified Lucas Washburn equation [37] are given in Table B1.

Table B1. CA capillary flow parameters

γ (N/m)	ρ_h (kg/m^3)	μ (Ns/m^2)	θ_s (rad)	β_s (-)	β_m (Ns/m^2)	β_w (m^3/Ns)
0.033	1060	0.004	0.175	0.01	0.55	0.0025

in which γ is the surface tension, ρ_h is the density, μ is the viscosity, θ_s is the static contact angle, β_s *is the* stick-slip parameter, β_m is the meniscus frictional dissipation parameter and β_w is the wall slip parameter.

Sorption parameters

The sorption of CA into a block of concrete through a crack face was measured in a series of tests and the response simulated with the following sorption function;

$$h_{cap} = -\frac{\sqrt{\pi}\, S\, erfc\left(\sqrt{t/\tau}\right)}{2\sqrt{1/\tau}} + \frac{\sqrt{\pi}\, S}{2\sqrt{1/\tau}} \tag{B1}$$

in which t is time, h_{cap} is the capillary rise height, $erfc(x)$ is the complimentary error function, S is the sorption coefficient and τ the sorption time parameter.

From this study, the mean value of S = 0.48 mm/s$^{1/2}$ with a CoV of 16.67 % and τ = 50s.

Curing front parameters

It was shown in [51] that a curing front develops and progresses in the body of CA adjacent to a cementitious substrate (i.e. concrete crack surface) according to the following equation:

$$z_c(t) = z_{c0}\left(1 - e^{\frac{-t}{\tau_c}}\right) \tag{B2}$$

where z_c is the curing front position, relative to the substrate, z_{c0} is a critical curing depth and τ_c is a curing time parameter.

The mean value of z_{c0} = 1.25 with CoV=16% and τ_c = 300s

Dynamic capillary flow parameters

The following formula of Bracke et al. [76] was shown to be applicable to the dynamic flow of CA and was calibrated using data from a set of dynamic flow tests;

$$\theta_d = arccos\left(cos\theta_s - \mathrm{C}_1(1 + cos\theta_s)C_a{}^{\mathrm{C}_2}\right) \tag{B3}$$

in which θ_d is the dynamic contact angle, and the constants C_1 and C_2 were calibrated to be 0.8621 and 0.1947 respectively.

A representation CoV from the four experimental series used to determine C_1 and C_2 is 10% (See ref [51])

REFERENCES

[1] D. Gardner, R. Lark, T. Jefferson, R. Davies, A survey on problems encountered in current concrete construction and the potential benefits of self-healing cementitious materials, Case Stud. Constr. Mater. 8 (2018) 238–247. doi:10.1016/j.cscm.2018.02.002.

[2] N. De Belie, E. Gruyaert, A. Al-Tabbaa, P. Antonaci, C. Baera, D. Bajare, A. Darquennes, R. Davies, L. Ferrara, T. Jefferson, C. Litina, B. Miljevic, A. Otlewska, J. Ranogajec, M. Roig-Flores, K. Paine, P. Lukowski, P. Serna, J.M. Tulliani, S. Vucetic, J. Wang, H.M. Jonkers, A Review of Self-Healing Concrete for Damage Management of Structures, Adv. Mater. Interfaces. 5 (2018) 1–28. doi:10.1002/admi.201800074.

[3] T. Jefferson, E. Javierre, B. Freeman, A. Zaoui, E. Koenders, L. Ferrara, Research Progress on Numerical Models for Self-Healing Cementitious Materials, Adv. Mater. Interfaces. 5 (2018) 1–19. doi:10.1002/admi.201701378.

[4] C. Xue, W. Li, J. Li, V.W.Y. Tam, G. Ye, A review study on encapsulation-based self-healing for cementitious materials, Struct. Concr. 20 (2019) 198–212. doi:10.1002/suco.201800177.

[5] K. Van Tittelboom, N. De Belie, Self-healing in cementitious materials-a review, 2013. doi:10.3390/ma6062182.

[6] C. Joseph, A.D. Jefferson, B. Isaacs, R. Lark, D. Gardner, Experimental investigation of adhesive-based self-healing of cementitious materials, Mag. Concr. Res. 62 (2010) 831–843. doi:10.1680/macr.2010.62.11.831.

[7] C. De Nardi, A. Cecchi, L. Ferrara, A. Benedetti, D. Cristofori, Effect of age and level of damage on the autogenous healing of lime mortars, Compos. Part B Eng. 124 (2017) 144–157. doi:10.1016/j.compositesb.2017.05.041.

[8] D.J. Kim, S.H. Kang, T.H. Ahn, Mechanical Characterization of High-Performance Steel-Fiber Reinforced Cement Composites with Self-Healing Effect, Materials (Basel). 7 (2014) 508–526. doi:10.3390/ma7010508.

[9] V.C. Li, Y.M. Lim, Y.W. Chan, Feasibility study of a passive smart self-healing cementitious composite, Compos. Part B Eng. 29 (1998) 819–827. doi:10.1016/S1359-8368(98)00034-1.

[10] C. Dry, Matrix cracking repair and filling using active and passive modes for smart timed release of chemicals from fibers into cement matrices, Smart Mater. Struct. 3 (1994) 118–123. doi:10.1088/0964-1726/3/2/006.

[11] H. Mihashi, Y. Kaneko, T. Nishiwaku, K. Otsuka, Fundamental study on development of intelligent concrete characterized by self-healing capability for strength, Trans. Jpn Concr. Inst. 22 (2000) 441-450.

[12] J. Wang, K. Van Tittelboom, N. De Belie, W. Verstraete, Use of silica gel or polyurethane immobilized bacteria for self-healing concrete, Constr. Build. Mater. 26 (2012) 532–540. doi:10.1016/j.conbuildmat.2011.06.054.

[13] P. Minnebo, G. Thierens, G. De Valck, K. Van Tittelboom, N. De Belie, D. Van Hemelrijck, E. Tsangouri, A novel design of autonomously healed concrete: Towards a vascular healing network, Materials (Basel). 10 (2017) 1–23. doi:10.3390/ma10010049.

[14] M. Araújo, S. Chatrabhuti, S. Gurdebeke, N. Alderete, K. Van Tittelboom, J.M. Raquez, V. Cnudde, S. Van Vlierberghe, N. De Belie, E. Gruyaert, Poly(methyl methacrylate) capsules as an alternative to the proof-of-concept'' glass capsules used in self-healing concrete, Cem. Concr. Compos. 89 (2018) 260–271. doi:10.1016/j.cemconcomp.2018.02.015.

[15] L. Sun, W. Yu, Q. Ge, Experimental research on the self-healing performanace of micro-cracks in concrete bridge, Adv. Mater. Res. 250 (2011) 28-32.

[16] H. Huang, G. Ye, Z. Shui, Feasibility of self-healing in cementitious materials - By using capsules or a vascular system?, Constr. Build. Mater. 63 (2014) 108–118. doi:10.1016/j.conbuildmat.2014.04.028.

[17] M. Pelletier, Smart Concrete. https://www.archdaily.com/62357/smart-concrete-michelle-pelletier (accessed 5 June 2019).

[18] H. Huang, G. Ye, Application of sodium silicate solution as self-healing-agent in cementitious materials, in: C. Leung, K.T. Wan (Eds.), Int. RILEM Conf. Adv. Constr. Mater. Through Sci. Eng., RILEM Publications SARL, (2011) 530–536.

[19] E. Mostavi, S. Asadi, M.M. Hassan, M. Alansari, Evaluation of self-healing mechanisms in concrete with double-walled sodium silicate microcapsules, J. Mater. Civ. Eng. (2015). p. 04015035.

[20] A. Beglarigale, Y. Seki, N.Y. Demir, H. Yazıcı, Sodium silicate/polyurethane microcapsules used for self-healing in cementitious materials: Monomer optimization, characterization, and fracture behavior, Constr. Build. Mater. 162 (2018) 57–64. doi:10.1016/j.conbuildmat.2017.11.164.

[21] K. Van Tittelboom, N. De Belie, D. Van Loo, P. Jacobs, Self-healing efficiency of cementitious materials containing tubular capsules filled with healing-agent, Cem. Concr. Compos. 33 (2011) 497–505. doi:10.1016/j.cemconcomp.2011.01.004.

[22] M. Maes, K. Van Tittelboom, N. De Belie, The efficiency of self-healing cementitious materials by means of

encapsulated polyurethane in chloride containing environments, Constr. Build. Mater. 71 (2014) 528–537. doi:10.1016/j.conbuildmat.2014.08.053.

[23] F.A. Gilabert, K. Van Tittelboom, J. Van Stappen, V. Cnuddle, N. De Belie, W. Van Paepegem, Integral procedure to assess crack filling and mechanical contribution of polymer-based healing-agent in encapsulation-based self-healing concrete, Cem. Concr. Compos. 77 (2017) 68-80. doi.org/10.1016/j.cemconcomp.2016.12.001.

[24] K. Van Tittelboom, J. Wang, M. Araújo, D. Snoeck, E. Gruyaert, B. Debbaut, H. Derluyn, V. Cnudde, E. Tsangouri, D. Van Hemelrijck, N. De Belie, Comparison of different approaches for self-healing concrete in a large-scale lab test, Constr. Build. Mater. 107 (2016) 125–137. doi:10.1016/j.conbuildmat.2015.12.186.

[25] J. Feiteira, E. Tsangouri, E. Gruyaert, C. Lors, G. Louis, N. De Belie, Monitoring crack movement in polymer-based self-healing concrete through digital image correlation, acoustic emission analysis and SEM in-situ loading, Mater. Des. 115 (2017) 238–246. doi:10.1016/j.matdes.2016.11.050.

[26] J. Hu, Q. Ren, Q. Jiang, R. Gao, L. Zhang, Z. Luo, Strength Characteristics and the Reaction Mechanism of Stone Powder Cement Tailings Backfill, Adv. Mater. Sci. Eng. 2018 (2018) 1–14. doi:10.1155/2018/8651239.

[27] C. Dry, W. McMillan, Three-part methylmethacrylate adhesive system as an internal delivery system for smart responsive concrete, Smart Mater. Struct. 5 (1996) 297–300. doi:10.1088/0964-1726/5/3/007.

[28] K. Van Tittelboom, K. Adesanya, P. Dubruel, P. Van Puyvelde, N. De Belie, Methyl methacrylate as a healing-agent for self-healing cementitious materials, Smart Mater. Struct. 20 (2011). doi:10.1088/0964-1726/20/12/125016.

[29] Q. Li, Siddaramaiah, N.H. Kim, D. Hui, J.H. Lee, Effects of dual component microcapsules of resin and curing agent on the self-healing efficiency of epoxy, Compos. Part B Eng. 55 (2013) 79–85. doi:10.1016/j.compositesb.2013.06.006.

[30] W. Li, Z. Jiang, Z. Yang, Acoustic characterization of damage and healing of microencapsulation-based self-healing cement matrices, Cem. Concr. Compos. 84 (2017) 48–61. doi:10.1016/j.cemconcomp.2017.08.013.

[31] G. Perez, E. Erkizia, J.J. Gaitero, I. Kaltzakorta, I. Jiménez, A. Guerrero, Synthesis and characterization of epoxy encapsulating silica microcapsules and amine functionalized silica nanoparticles for development of an innovative self-healing concrete, Mater. Chem. Phys. 165 (2015) 39–48. doi:10.1016/j.matchemphys.2015.08.047.

[32] S.R. White, N.R. Sottos, P.H. Geubelle, J.S. Moore, M.R. Kessler, S.R. Sriram, E.N. Brown, S. Viswanathan, Autonomic healing of polymer composites, Nature. 409 (2001) 794–797. doi:10.1038/35057232.

[33] Z. Yang, J. Hollar, X. He, X. Shi, A self-healing cementitious composite using oil core/silica gel shell microcapsules, Cem. Concr. Compos. 33 (2011) 506–512. doi:10.1016/j.cemconcomp.2011.01.010.

[34] X. Wang, F. Xing, M. Zhang, N. Han, Z. Qian, Experimental study on cementitious composites embedded with organic microcapsules, Materials (Basel). 6 (2013) 4064–4081. doi:10.3390/ma6094064.

[35] A. Kanellopoulos, P. Giannaros, D. Palmer, A. Kerr, A. Al-Tabbaa, Polymeric microcapsules with switchable mechanical properties for self-healing concrete: synthesis, characterisation and proof of concept, Smart Mater. Struct. 26 (4) (2017) 045025. doi:10.1088/1361-665X/aa516c.

[36] L. Souza, A. Al-Tabbaa, Microfluidic fabrication of microcapsules tailored for self-healing in cementitious materials, Constr. Build. Mater. 184 (2018) 713–722. doi:10.1016/j.conbuildmat.2018.07.005.

[37] D. Gardner, A. Jefferson, A. Hoffman, R. Lark, Simulation of the capillary flow of an autonomic healing-agent in discrete cracks in cementitious materials, Cem. Concr. Res. 58 (2014) 35–44. doi:10.1016/j.cemconres.2014.01.005.

[38] B. Van Belleghem, K. Van Tittelboom, N. De Belie, Efficiency of self-healing cementitious materials with encapsulated polyurethane to reduce water ingress through cracks, Materiales de Construcción 68 (2018). doi: 10.3989/mc.2018.05917.

[39] A. Formia, S. Terranova, P. Antonaci, N.M. Pugno, J.M. Tulliani, Setup of extruded cementitious hollow tubes as containing/releasing devices in self-healing systems, Materials (Basel). 8 (2015) 1897–1923. doi:10.3390/ma8041897.

[40] Y. Kuang, J. Ou, Self-repairing performance of concrete beams strengthened using superelastic SMA wires in combination with adhesives released from hollow fibers, Smart Mater. Struct. 17 (2008). doi:10.1088/0964-1726/17/2/025020.

[41] C. Dry, M. Corsaw, E. Bayer, A comparison of internal self-repair with resin injection in repair of concrete, J. Adhes. Sci. Technol. 17 (2003) 79–89. doi:10.1163/15685610360472457.

[42] S. Pareek, K.C. Shrestha, Y. Suzuki, T. Omori, R. Kainuma, Y. Araki, Feasibility of externally activated self-repairing concrete with epoxy injection network and Cu-Al-Mn superelastic alloy reinforcing bars, Smart Mater.

Struct. 23 (2014). doi:10.1088/0964-1726/23/10/105027.

[43] R. Davies, A. Jefferson, R. Lark, D. Gardner, A Novel 2D Vascular Network in Cementitious Materials, Concr. – Innov. Des. Fib Symp. Copenhagen May 18-20, 2015 A. (2015) 1–7. doi:10.1177/1753193414554772.

[44] R. Davies, O. Teall, M. Pilegis, A. Kanellopoulos, T. Sharma, A. Jefferson, D. Gardner, A. Al-Tabbaa, K. Paine, R. Lark, Large Scale Application of Self-Healing Concrete: Design, Construction, and Testing, Front. Mater. 5 (2018) 1–12. doi:10.3389/fmats.2018.00051.

[45] L. Ferrara, T. Van Mullem, M.C. Alonso, P. Antonaci, R.P. Borg, E. Cuenca, A. Jefferson, P.L. Ng, A. Peled, M. Roig-Flores, M. Sanchez, C. Schroefl, P. Serna, D. Snoeck, J.M. Tulliani, N. De Belie, Experimental characterization of the self-healing capacity of cement based materials and its effects on the material performance: A state of the art report by COST Action SARCOS WG2, Constr. Build. Mater. 167 (2018) 115–142. doi:10.1016/j.conbuildmat.2018.01.143.

[46] A. Sidiq, R. Gravina, F. Giustozzi, Is concrete healing really efficient? A review, Constr. Build. Mater. 205 (2019) 257–273. doi:10.1016/j.conbuildmat.2019.02.002.

[47] T.S. Qureshi, A. Kanellopoulos, A. Al-Tabbaa, Encapsulation of expansive powder minerals within a concentric glass capsule system for self-healing concrete, Constr. Build. Mater. 121 (2016) 629–643. doi:10.1016/j.conbuildmat.2016.06.030.

[48] D. Snoeck, N. De Belie, Mechanical and self-healing properties of cementitious composites reinforced with flax and cottonised flax, and compared with polyvinyl alcohol fibres, Biosyst. Eng. 111 (2012) 325–335. doi:10.1016/j.biosystemseng.2011.12.005.

[49] S. Liu, Z.B. Bundur, J. Zhu, R.D. Ferron, Evaluation of self-healing of internal cracks in biomimetic mortar using coda wave interferometry, Cem. Concr. Res. 83 (2016) 70–78. doi:10.1016/j.cemconres.2016.01.006.

[50] B. Freeman and A. Jefferson, The simulation of transport processes in cementitious materials with embedded healing systems. International Journal for Numerical and Analytical Methods in Geomechanics (2019) 1–34. doi:10.1002/nag.3017.

[51] T. Selvarajoo, R. E. Davies, D. R. Gardner, B. L. Freeman, A. D. Jefferson, Characterisation of a vascular self-healing cementititous material system: flow and curing properties. Construction and Building Materials 245 (2020) 118332. doi.org/10.1016/j.conbuildmat.2020.118332

[52] Cyanotec, Technical Data Sheet for Procure PC20. http://www.gluesdirect.co.uk/catalog/product_info.php?products_id=151, 2016 (accessed 5th January 2020).

[53] S.K. Tomlinson, O.R. Ghita, R.M. Hooper, K.E. Evans, The use of near-infrared spectroscopy for the cure monitoring of an ethyl cyanoacrylate adhesive, Vib. Spectrosc. 40 (2006) 133–141. doi:10.1016/j.vibspec.2005.07.009.

[54] M. Ait Ouarabi, P. Antonaci, F. Boubenider, A.S. Gliozzi, M. Scalerandi, Ultrasonic Monitoring of the Interaction between Cement Matrix and Alkaline Silicate Solution in Self-Healing Systems. Materials 2017, 10(1), 46. doi: 10.3390/ma10010046.

[55] L. Jiang, X. Xue, W. Zhang, J. Yang, H. Zhang, Y. Li, R. Zhang, Z. Zhang, L. Xu, J. Qu, J. Song, J. Qin, The investigation of factors affecting the water impermeability of inorganic sodium silicate-based concrete sealers. Constr. Build. Mater. 2015, 93, 729-736. doi: 10.1016/j.conbuildmat.2015.06.001

[56] A. M. Neville, Properties of Concrete, fifth ed., Prentice Hall, London, 2012.

[57] D.R. Gardner, R.J. Lark, B. Barr, Effect of conditioning temperature on the strength and permeability of normal- and high-strength concrete, Cem. Concr. Res. 35 (2005) 1400–1406. doi:10.1016/j.cemconres.2004.08.012.

[58] A.K. Schindler and K.J. Folliard, Heat of hydration models for cementitious materials, ACI Journal, 2005, 24-33.

[59] H. W. Reinhardt, Similitude of brittle fracture of structural concrete, Adv. Mech. of Reinforced Conc. (1981) 69-92. doi:10.5169/seals-26886.

[60] J. C. W. van Mier, Fracture processes of concrete, first ed., CRC Press, London, 1997.

[61] J.S. Jacobsen, P.N. Poulsen, J.F. Olesen, Characterization of mixed mode crack opening in concrete, Mater. Struct. Constr. 45 (2012) 107–122. doi:10.1617/s11527-011-9754-5.

[62] T. Selvarajoo, Characterisation of a vascular self-healing cementititous material system (PhD thesis), Cardiff University, UK, 2019.

[63] E.J. Barbero, F. Greco, P. Lonetti, Continuum Damage-Healing Mechanics with application to self-healing composites, Int. J. Damage Mech. 14 (2005) 51–81. doi:10.1177/1056789505045928.

[64] E.C. Schimmel, J. Remmers, Development of a constitutive model for self-healing materials, Delft Aerosp. Comput. Sci. (2006) 17. https://repository.tudelft.nl/islandora/object/uuid%3A6ad6ebfd-aa1c-46f1-a9d5-

c17109b8a423.

[65] J. Mergheim, P. Steinmann, Phenomenological modelling of self-healing polymers based on integrated healing-agents, Comput. Mech. 52 (2013) 681–692. doi:10.1007/s00466-013-0840-0.

[66] G. Alfano, E. Sacco, Combining interface damage and friction in a cohesive-zone model, Int. J. Numer. Methods Eng. 68 (2006) 542–582. doi:10.1002/nme.1728.

[67] A.D. Jefferson, I.C. Mihai, The simulation of crack opening-closing and aggregate interlock behaviour in finite element concrete models, Int. J. Numer. Methods Eng. 104 (2015) 48–78. doi:10.1002/nme.4934.

[68] B. L. Karihaloo, Fracture mechanics and structural concrete, Longman Scientific & Technical, New York, 1995.

[69] V. Gopalaratnam, S. Shah, Softening response of plain concrete in direct tension, Struct. J. ACI, 82 (1985) 310-323. doi :10.14359/10338.

[70] D. Homma, H. Mihashi, T. Nishiwaki, Self-Healing Capability of Fibre Reinforced Cementitious Composites, J. Adv. Concr. Technol. 7 (2009) 217–228. doi:10.3151/jact.7.217.

[71] L. Ferrara, V. Krelani, M. Carsana, A “fracture testing” based approach to assess crack healing of concrete with and without crystalline admixtures, Constr. Build. Mater. 68 (2014) 535–551. doi:10.1016/j.conbuildmat.2014.07.008.

[72] H. Huang, G. Ye, D. Damidot, Characterization and quantification of self-healing behaviors of microcracks due to further hydration in cement paste, Cem. Concr. Res. 52 (2013) 71–81. doi:10.1016/j.cemconres.2013.05.003.

[73] R. Gettu, Z. Bazant, Rate Effects and Load Relaxation in Static Fracture of Concrete, ACI Mater. J. (1993) 456–468.

[74] M4L (2019) Cardiff University Database. http://doi.org/10.17035/d.2019.0081928129.

[75] A.D. Jefferson, B.I.G. Barr, T. Bennett, S.C. Hee, Three dimensional finite element simulations of fracture tests using the Craft concrete model, Comput. Concr. 1 (2004) 261–284. doi:10.12989/cac.2004.1.3.261.

[76] M. Bracke, F. De Voeght, P. Joos, The kinetics of wetting: the dynamic contact angle, Prog. Colloid Polym. Sci. 79 (1989) 142-149.